tion coefficient $\alpha$, which is calculated from a model similar to Ref. 4 without the polarization sensitivity.

It is interesting to note that the magnitude of $\Delta T$ (between F = 0 and 50 kV/cm) is enhanced in the DFQW ($L_d$ = 50 Å) for all values of R, as compared to the $L_d = 0$ case, at a chosen operational wavelength $\lambda_{op}$ = 758 nm (to obtain maximum $\Delta T$'s), see Fig. 2. Analysis of the modulator is based on the non-normalized $\Delta T/T$ spectra in the normal-OFF operational mode with an optimized R = 0.5 for the two $L_d$'s, see Fig. 3. One positive peak

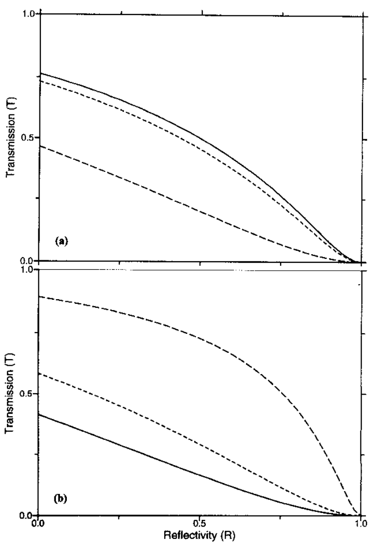


**P69 Fig. 2.** The transmission T spectra as a function of reflectivity R for F (kV/cm) = 0 (solid), 30 (dot), 50 (dash). (a) Ld = 0 Å at $\lambda_{op}$ = 0.850 μm and (b) Ld = 40 Å at $\lambda_{op}$ = 0.758 μm.

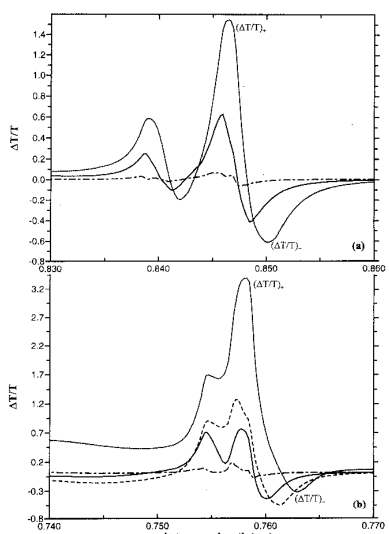


**P69 Fig. 3.** The $\Delta T/T$ spectra for DFQWs of thickness d = 0.5 μm and R = 0.5 for F (kV/cm) = 10 (dash-dot), 30 (solid), 40 (dash), and 50 (dot). (a) Ld = 0 Å and (b) Ld = 40 Å.

$(\Delta T/T)_+$ and one negative trough $(\Delta T/T)_-$ can be observed in each spectrum, where the former corresponds to the largest modulation depth while the latter, although slightly smaller in magnitude, corresponds to a lower resident absorption $\alpha(F = 0)$. It can be seen that $(\Delta T/T)_+$ increases from 1.53 ($L_d$ = 0) to 3.40 ($L_d$ = 40 Å), which is an attractive feature for developing a high intensity modulator with a narrow $\lambda_{op}$ range. Also a steady $\Delta T/T \cong 0.6$ (without any sign change) is obtained for a range of $\lambda_{op}$'s (740 to 760 nm ≅ 20 nm) in the DFQW between F = 40 and 50 kV/cm, therefore it can be operated as a 20 nm band-width transmission modulator with only a single DFQW structure. Finally, the $(\Delta T/T)_-$ has a wavelength range of $\lambda_{op} = 850 - 782 \cong 80$ nm with an acceptable fluctuation of $\Delta T/T = (0.62 - 0.54)/0.62 \cong 12\%$ for cases of $L_d$ from 0 to 30 Å, so it can be employed as a wide band-width modulator with a multi-section consists of differential $L_d$'s.

1. G. A. Evan, *et al.*, IEEE J. of Quantum Electron. **27**, 1594 (1991).
2. M. Whitehead, G. Parry, P. Wheatley, IEE Proc. Pt. J **136**, 52 (1989).
3. E. H. Li, B. L. Weiss, Phys. Rev. B **4**, 445 (1993).
4. E. H. Li, K. S. Chan, B. L. Weiss, J. Micallef, Appl. Phys. Lett. **63**, 533 (1993).

## P70

### Impurity induced disordering produced lateral optical confinement in AlGaAs/GaAs quantum well waveguides

E. Herbert Li, Chun-Bong Cheung, Wai-Kin Tsui, *Department of Electrical and Electronic Engineering, The University of Hong Kong, Pokfulam Road, Hong Kong*

The impurity induced disordering (IID) technique provides an efficient way to realize waveguiding structure in optoelectronic integrated circuits.[1] The masked implantation process produces a modification of the quantum well (QW) material which in turn modifies its refractive index.[2] This creates a refractive index step between the implanted and nonimplanted regions and produces lateral confinement for photons in the lateral dimension, thus a 2-D waveguide is formed. Although there have been a lot of effort spent in studying the electronic and optical properties of the IID modified AlGaAs/GaAs QW structures, the detailed waveguiding properties of this type of devices is still not known. A detail model is considered here on the two dimensional IID waveguide structure and results indicate guiding requirements on the structure's dimension, effects on the optical confinement factor, and the wavelength requirement for single mode propagation.

The structure to be modeled consists of $Al_{0.3}Ga_{0.7}As/GaAs$ QWs (10 to 40 periods of 100 Å wide well and barrier layers) and thick $Al_{0.3}Ga_{0.7}As$ buffer layer grown on a GaAs substrate; the schematic of the structure is shown in Fig. 1. In our model, $Ga^+$ ion is implanted with a projected range located around the center of the QW layers. The annealing time and temperature in the simulation is 20

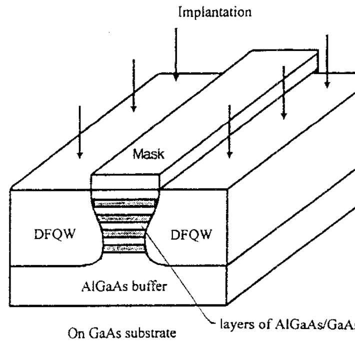


**P70 Fig. 1.** Schematic of the IID multi-quantum well waveguide structure.

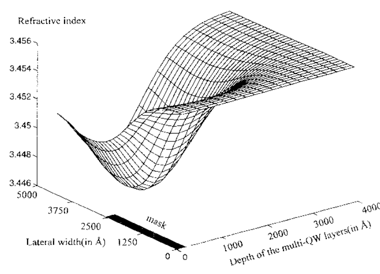


**P70 Fig. 2.** Refractive index profile (half symmetry) of a structure with 20 multi-QW layers, 5000 Å mask width, and propagation wavelength at 1 μm.

seconds and 900°C, respectively. In order to analyze the waveguiding properties accurately, the impurity density profile as-implanted was computed base on both experimental and simulation results.[3] On the basis of these initial conditions, the 2-D impurity distribution after an annealing time t was then computed by solving a non-constant coefficient diffusion equation using a finite element method. This impurity concentration profile determines the 2-D dependent diffusion coefficient and thus the position dependent diffusion length of the Al/Ga atoms at any given time can be obtained. Using a previously developed model,[4] a 2-D refractive index profile was then calculated from these diffusion lengths, as shown in Fig. 2. The TE mode waveguide equation was solved using a finite difference method to determine the propagation coefficient, $\beta$, as well as the optical electric field profile, and followed by the determination of the optical confinement factor.

The parameters of the IID waveguide structure such as the mask width, $L_M$, QW layer thickness, d, ion implantation energy, operational wavelengths, $\lambda$, were varied in order to analyze the single and multiple mode waveguiding requirements. It is found that the waveguide dimension, that is the mask width and the thickness of the multi-QW layers, should be at least half of the dimension of the propagation wavelength to provide a satisfactory wave confinement factor of ~0.5. In fact guiding was found to be sup-

Posters

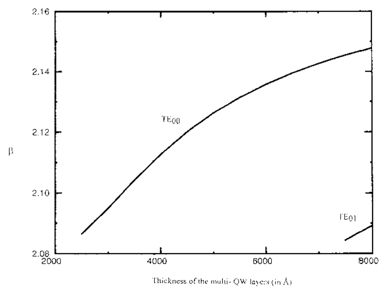


**P70 Fig. 3.** The propagation constant, β, as a function the thickness of the multi-QW layers, with mask width equals 5000 Å and propagation wavelength at 1 μm.

ported from d = 2200 Å up to 7500 Å for single mode and beyond for multiple mode with $L_M$ = 5000 Å at λ = 1 μm, see Fig. 3. The effect of $L_M$ (5000 Å to 10,000 Å) on the single mode properties remains unaffected for d = 4000 Å at λ = 1 μm, as is the variation of λ (0.8 to 1.55 μm) for d = 4000 Å and $L_M$ = 5000 Å.


1. See the special issue *Quantum well mixing for optoelectronics*, B. L. Weiss, Editor, Opt. Quantum Electron. **23**, s799–s994 (1991).
2. T. Wolf, C. L. Shieh, R. Engelmann, K. Alavi, J. Mantz, "Lateral refractive index step in GaAs/AlGaAs multiple quantum well waveguides fabricated by impurity-induced disordering," Appl. Phys. Lett. **55**, 1412–1414 (1989).
3. D. Briggs, M. P. Seah, Editors, *Practical Surface Analysis* (2nd Edition) **2**: Ion and Neutral Spectroscopy (Wiley, 1992).
4. E. H. Li, B. L. Weiss, K. S. Chan, J. Micallef, "Polarization dependent refractive index of an interdiffusion induced AlGaAs/GaAs quantum well," Appl. Phys. Lett. **62**, 550–552 (1992).


**P71**

## A simple and efficient scalar finite element approach to nonlinear optical channel waveguides

Akira Niiyama, Masanori Koshiba, *Department of Electronic Engineering, Hokkaido University, Kita-13, Nishi-8, Kita-ku, Sapporo 060, Japan*

Intensity-dependent phenomena in optical guiding structures have attracted much interest in recent years because of their potential use in all-optical processing. Most papers concerned with modal analysis of nonlinear optical waveguides have dealt with planar structures. Recently, a scalar finite element method (FEM) has been applied to modal analysis of nonlinear optical channel waveguides.[1,2] Although the scalar FEM is approximate in a strict sense, in contrast to the vector FEM,[2,3] this approach has as its main advantages: the smaller matrix dimensions, no spurious solutions, and capability of easily computing the propagation constant at a given frequency. In the earlier works,[1,2] however, only the TE-like wave propagation is considered, and the intensity-dependent refractive index is assumed to be constant within each element. Hence, if the accuracy of solutions needs to be improved, the scale of computation becomes significantly large.[1]

In this paper a unified approach based on the scalar FEM is developed for both TE-like and TM-like nonlinear waves in optical channel waveguides. In order to faithfully evaluate the intensity-dependent refractive index within each element according to the electric field distributions and to treat arbitrarily shaped nonlinear optical waveguides, quadratic isoparametric curvilinear elements and numerical integration formulae derived by Hammer *et al.*[4] are introduced. Propagation characteristics of nonlinear elliptical core optical fibers and graded-index nonlinear optical channel waveguides are investigated for the first time.

Fig. 1 shows power dispersion curves for an elliptical core optical fiber with

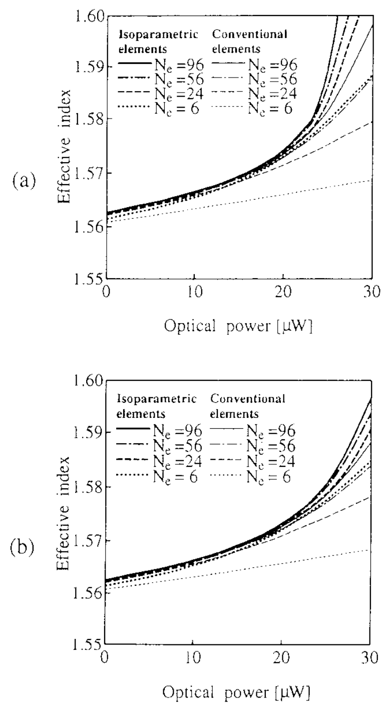


**P71 Fig. 1.** Power dispersion curves for an elliptical core optical fiber with Kerr nonlinearity in the core. (a) Fundamental TE-like mode. (b) Fundamental TM-like mode.

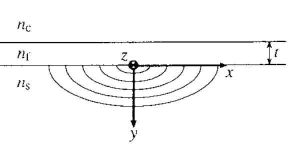


$$n_f = n_{f0} + \Delta n_{sat}\left[1 - \exp\left(-\frac{n_{f0}n'|E|^2}{2\Delta n_{sat}Z_0}\right)\right]$$

$$n_s = n_{s0} + \Delta n f(x/d_x)g(y/d_y)$$

**P71 Fig. 2.** Graded-index nonlinear optical channel waveguide.

Kerr nonlinearity in the core, a major axis of $\sqrt{2}$ μm, a minor axis of $1/\sqrt{2}$ μm, a core index of 1.57, a cladding index of 1.55, and a nonlinear-optical coefficient of $10^{-9}$ $m^2$/W, where the wavelength λ = 0.5145 μm and $N_e$ is the number of elements. In the present approach using isoparametric elements the convergence of solutions is very fast irrespective of the difference of polarizations. The modal birefringence is greatly enhanced with increasing optical power. We have confirmed that the results of the present approach for a circular core optical fiber are in good agreement with analytical solutions for axisymmetric structures.[5] It is interesting to note that the power dispersion curve for the TE-like mode of an elliptical core fiber with a major axis of $\sqrt{2}$ μm and a minor axis of $1/\sqrt{2}$ μm is similar to that for the $LP_{01}$ mode of a circular core fiber with the same core area, namely, a core diameter of 1 μm.

Next, we consider a graded-index optical channel waveguide as shown in Fig. 2, where λ = 0.515 μm, $t$ = 1.0 μm, $n_{f0}$ = 1.55, $n_{s0}$ = 1.55, $n_{c0}$ = 1.0, $\Delta n$ = 0.02, $\Delta n_{sat}$ = 0.04, $n'$ = $10^{-9}$ $m^2$/W, diffusion lengths $d_x = d_y$ = 3 μm, and the saturable nonlinearity is assumed. Fig. 3 shows power dispersion curves for various types of nonlinear optical channel waveguides: type 1 with Gaussian and exponential profiles in the $x$ and $y$ directions, type 2 with Gaussian profiles in both directions, and type 3 with step-index profiles in both directions. The dispersion curves exhibit switching and hysteresis natures, and the threshold power becomes higher and the width of the hysteresis loop be-

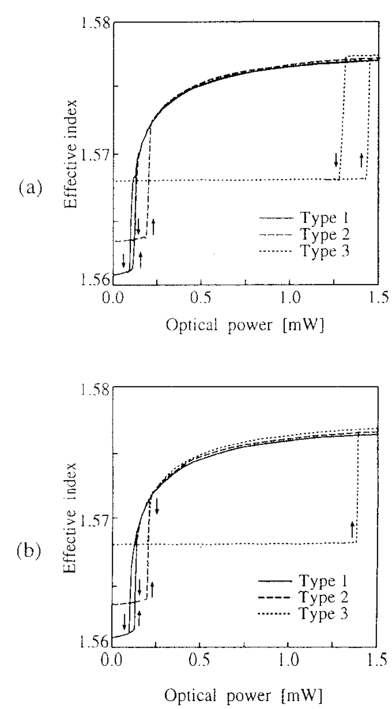


**P71 Fig. 3.** Power dispersion curves for a graded-index nonlinear optical channel waveguide. (a) Fundamental TE-like mode. (b) Fundamental TM-like mode.

Posters